View metadata, citation and similar papers at core.ac.uk

brought to you by CORE

provided by KHALSA PUBLICATIONS

ISSN 2347-3487

Hadronization properties in e^+e^- annihilation at $\sqrt{S} = 60$ GeV centre of mass energy

M.E. Zomorrodian1* ,M. Hasheminia2, A. Mirjalili2

1- Department of physics,Ferdowsi University of Mashhad, 91775-1436, Mashhad, Iran.

2-Faculty of Physics, University of Yazd, P.O.Box 89195-741 Yazd, Iran

*Corresponding author: zomorrod@um.ac.ir

ABSTRACT

The hadronic events from the experimental data, as well as the PYTHIA Monte-carlo data at the 60 GeV centre of mass energies are studied.We present the general properties of multihadron final states produced by e^+e^-.Global shape, inclusive charged-particle, and particle-flow distributions are presented. Our measurements are compared with QCD + fragmentation models that use either leading-logarithmic parton-shower evolution or QCD matrix elements at the parton level, and either string or cluster fragmentation for hadronization. Possible explanations for ourcompariaon are presented in this paper.

Key words: QCD models; hadronization; fragmentation.

Council for Innovative Research

Peer Review Research Publishing System

Journal: JOURNAL OF ADVANCES IN PHYSICS

Vol 5, No.2

japeditor@gmail.com

www.cirjap.com

ISSN 2347-3487

1. INTRODUCTION

Quantum chromodynamics (QCD) [1-3], the gauge theory of colored quarks and gluons, was introduced to explain the properties of hadrons. QCD has subsequently become the accepted theory of the strong interaction. However, it remains that the least quantitatively tested part of the so-called standard model of elementary-particle physics, i.e., the standard (Glashow-Salam-Weinberg) electroweak model and QCD [4]. In particular, the transition from partons to the observable hardons is, as yet, not well understood. There has been progress in recent years in the development of models of the process $e^+e^- \to \gamma^* / Z^* \to hadrons$ that generate partons according to perturbative QCD followed by a phenomenological hadronization scheme for the metamorphosis of the partons into hadrons. These QCD + fragmentation models have helped experimentalists to correct their data and plumb the underlying parton structure to provide a framework to understand better the long-range behavior of the strong interaction.

We compare in this paper our AMY as well as the PYTHIA Monte-Carlo simulated data to different QCD + fragmentation models. A brief description of the AMY detector is described in section 2. In Sec. 3 we describe the QCD + fragmentation models used for comparing our data. The definitions for global event-shape and inclusive particle properties are presented in Sec.4. Our physics results and comparison with different models are presented in sect. 5. The last section includes our conclusion.

2- Experimental set up

The central feature of the AMY detector is a 3-T solenoid magnet that allows the detector to be compact while maintaing good momentum resolution. Charged particles are detected efficiently over the polar angle region $cos\theta < 0.87$ with a momentum resolution $\Delta_{p_T} = 0.7\% \times \left[p_T(GeV/c)\right]$. The detailed description of the various detector components has been described elsewhere [13].

3. QCD+FRAGMENTATION MODELS

Present QCD + fragmentation models can in general be divided into two classes: those in which parton distributions are generated following leading-logarithm parton shower evolution and those in which they are produced according to QCD matrix elements. Fragmentation of the partons into hadrons follows, usually employing one of three mechanisms: string, cluster, or independent.

Because of their complexity, fragmentation models are now almost exclusively implemented via Monte Carlo techniques in computer programs. This also enables the experimenter to pass events generated by a particular model through a detector simulation allowing close comparison between models and data. In this paper, we compare AMY data distributions generated by three of the most widely used QCD + fragmentation model programs: the Lund JETSET program version 6.2, incorporating matrix-elements calculations and the Lund parton shower model in version 6.3 [5], both with string fragmentation, and the Marchesini-Webber parton shower and cluster-decay program BIGWIG 4.3. Important features of these models are briefly discussed below.

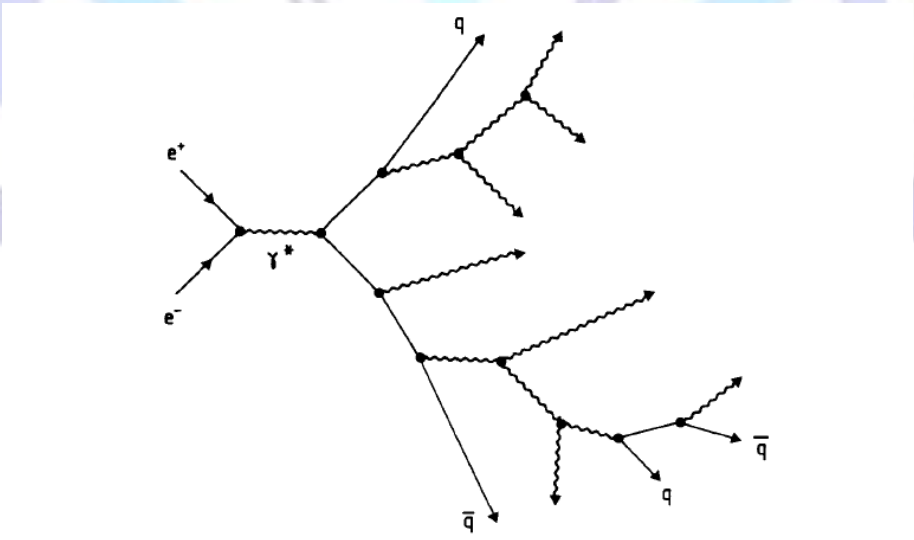

The branching process $e^+e^- \to q\bar{q}$ according to perturbative QCD

ISSN 2347-3487

A: **Lund Parton Shower Model (JETSET)[18-20]**.

In the Lund Parton Shower (PS) model (program JETSET version 7.4 [7, 8]), the evolution of the parton system is treated as a branching process based on the leading logarithmic approximation (LLA). In this picture partons undergo decays of the type $q \to qg$, $g \to gg$ and $g \to q\bar{q}$ The probability for the decay of a parton **a** with virtual mass m_a into partons ***b*** and ***c*** is given by the Altarelli-Parisi ("DGLAP") epuation :

$$\frac{dP_{a\to bc}}{dt} = \int dz \frac{\alpha_s\left(Q^2\right)}{2\pi} p_{a\to bc(z)}$$

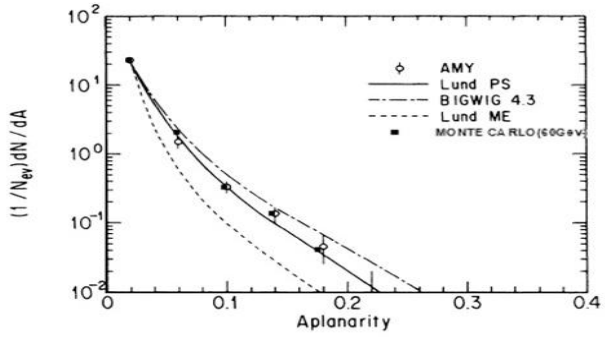

Fig 1: The aplanarity distributions and predictions of the models**.**

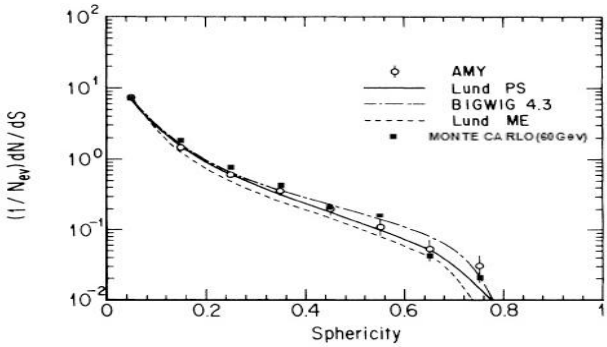

Fig 2: Sphericity distributions and predictions of the models.

where the evolution parameter *t* is related to the parent's virtual mass and to the QCD scale parameter Λ by $t = \ln\left(m_a^2/\Lambda^2\right)$. The strong coupling constant $\alpha_s\left(Q^2\right)$ is evaluated at (Q^2) equal to the transverse momentum squared of the branching. $P_{a\to bc}(z)$ is the Altarelli-Parisi splitting function. This function is also used to generate the energy fraction z and $1-z$ carried by the daughters. The decay angle is determined by two-body kinematics once the parent and daughter masses and energy fractions have been fixed.

For the first branchings of the initial quark and antiquark, an acceptance-rejection technique is applied so as to reproduce the three-jet cross section. Coherence effects are included by requiring that the emission angles of successive branching always decrease (angular ordering). Certain other higher order effects are also included, such as the azimuthal distribution in gluon decays from spin and coherence effects. The parton shower is stopped when the parton virtualities drop below a cut-off M_{min}

The conversion of the partons into hadrons is accomplished with the Lund String Model [5]. Gluons are associated with momentum carrying kinks in the string. Hadron production result from a breaking of the string which can be interpreted as virtual quark-antiquark pair production in a flux-tube. The quark's (equal and opposite) transverse momenta are generated according to a Gaussian distribution of width σ_{q*}. Longitudinal hadron momenta are determind by means of phenomenological fragmentation function: the Lund symmetric function with parameters *a* and *b* for light (u,d,s) quarks, and the Peterson function [10] with parameters ε_a and ε_b for *c* and *b* quarks.

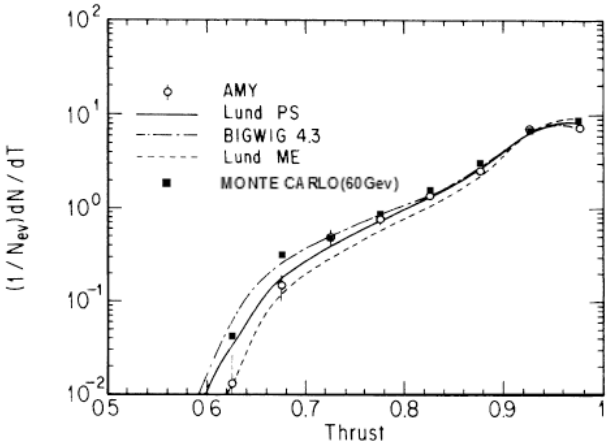

Fig 3: Thrust distributions and predictions of the models.

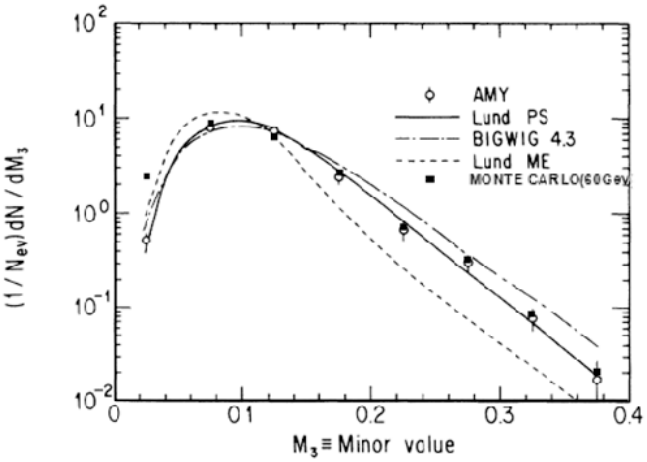

Fig 4: M_3 distributions and predictions of the models.

B:The Webber Model[21-22]

The Webber fragmentation scheme is incorporated into the programs BIGWIG and HERWIG Monte Carlo (version 5.8) [9] which is also based on a parton branching process, as described for JETSET. Instead of the parton virtual mass for the evolution parameter, HERWIG uses $t = \mathrm{In}\left(\zeta_a^2/\Lambda^2\right)$, where ζ_a is defined by

$$\zeta_a = E_a\sqrt{\xi_{bc}}, \qquad \xi_{bc} = \frac{P_b \cdot P_c}{E_b E_c}$$

for the branching $a \to bc$ where P_b, P_c, E_b and E_c are the four-momenta and energies of partons *b* and *c*. Angular ordering of successive branching is approximately equivalent to ordering of the ξ_{bc}. The argument *z* of the Altarelli-Parisi splitting function is taken to be the daughter's energy fraction and the scale for α_s is the transverse momentum squared of the branching. Azimuthal asymmetries for gluon decays both from coherence and spin effects are included. The treatment of hard gluon emission is improved by matching the parton shower cross section to the $O(\alpha_s)$ matrix element.

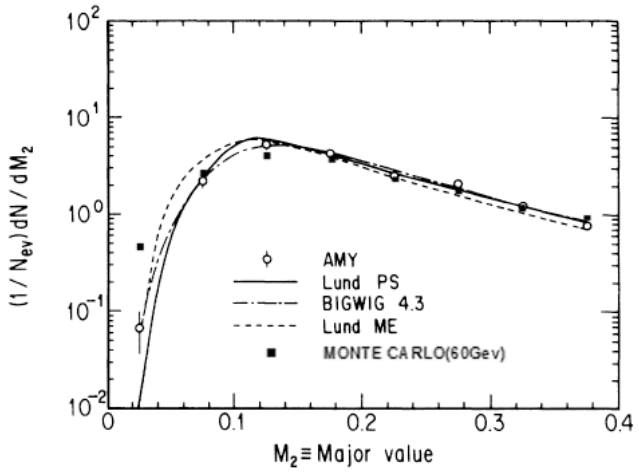

Fig 5: M_2 distributions and predictions of the models.

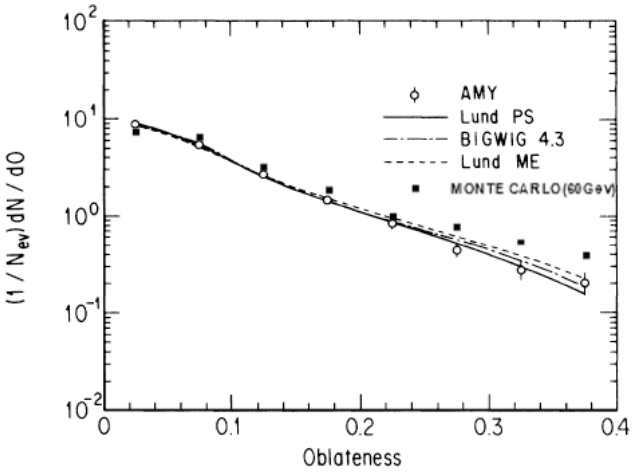

Fig 6: Oblateness distributions and predictions of the models.

ISSN 2347-3487

The hadronization in HERWIG is modeled with a cluster mechanism. At the end of parton shower, all gluons split into quark-antiquark pairs neighboring $q\bar{q}$ pairs from colour-neutral clusters which (usually) decay into two hardons. Special treatment is given to very light clusters, which are allowed to "decay" into a single hadron, and to very heavy cluster (mass> $m_{mass}^{cluster}$) which can decay further into clusters before decaying into hadrons. Baryons are produced from cluster decays into baryon-antibaryon pairs, i.e. clusters themselves always have baryon number of zero. If a cluster contains a quark that originated in the perturbative phase of the parton shower (i.e. not from the non-perturbative gluon splitting) then the angular distribution for the hadron that contains this quark is given by an exponential distribution .

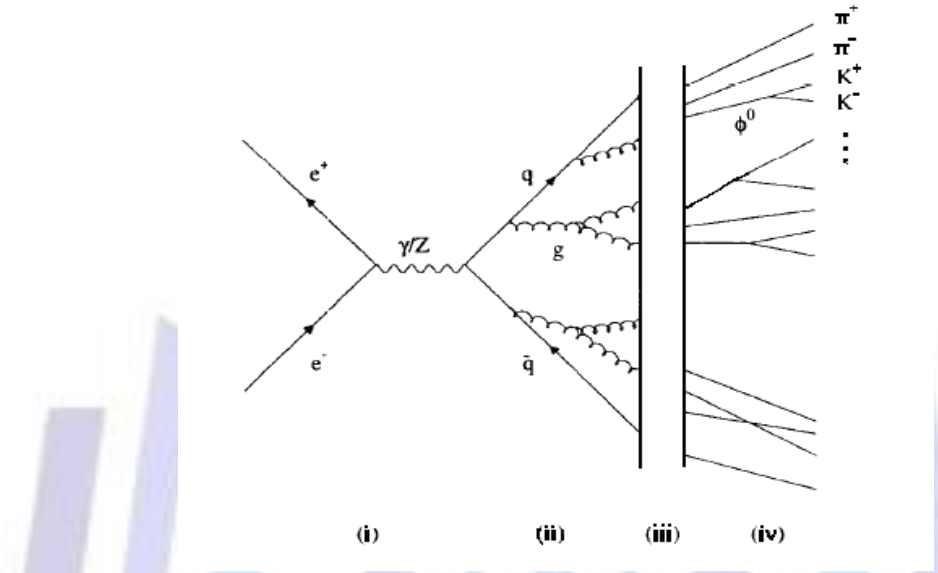

Schematic of hadronization in HERWIG.

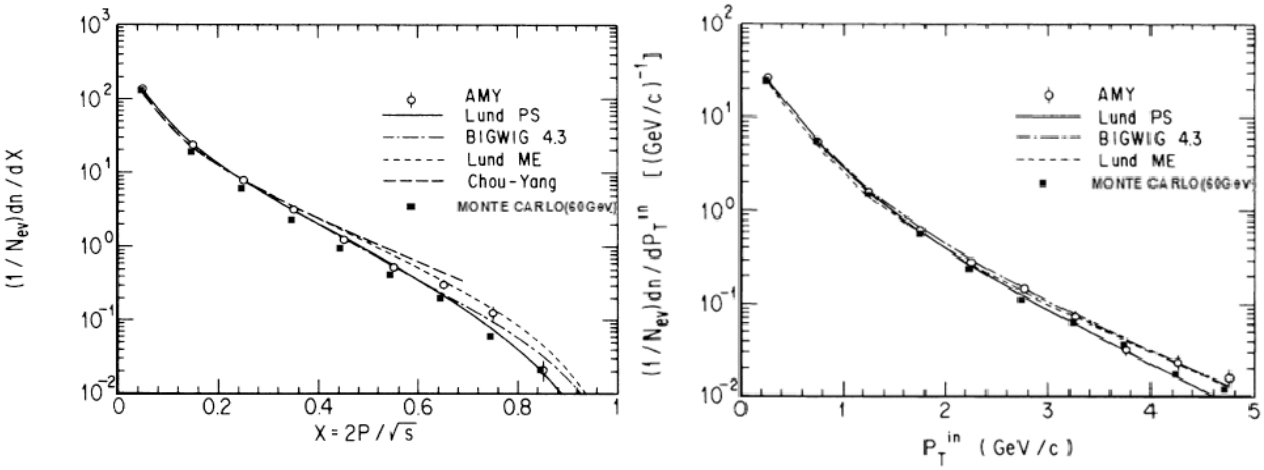

Fig 7: The X distributions and predictions of the models. **Fig 8:** P_T^{in} distributions and predictions of the models.

C:The Lund matrix-element model[23]

QCD matrix-element prediction for the production of two-, three-, and four-patron final states ($e^+e^- \to q\bar{q}, q\bar{q}g, q\bar{q}gg, q\bar{q}q\bar{q}$), calculated up to second order in α_s , are used by this model. To first order, the model uses

$$\alpha_s = \frac{12\pi}{(33-2n_f)\ln\left(Q^2/A_{\overline{MS}}^2\right)},$$

where n_f is the number of active flavors and $A_{\overline{ms}}$ is one of the parameters of the model ($\overline{MS}$ denotes the modified minimal-subtraction scheme). To avoid divergences in the Monte Carlo generation, three-parton events in which one parton is collinear or soft gluon are merged with the two-parton events. This cutoff is given in terms of the parameter y_{min}, which specifies the minimum required invariant mass squared of any two parton *i* and *j* in an event as fraction of *s*, the total center-of-mass energy squared $\left(M_{ij}^2 > y_{min} s\right)$ [15-17]. As has been observed the Lund matrix-element model, which allows states with at most four partons, fails to reproduce the rates for four or five-jet-like events. At lower energies, second-order matrix element appear to be sufficient, but this deficiency begins to become evident at PETRA and PEP energies. Because of the complexity of calculation to third order, simulation program which include higher order QCD contributions to jet cross section are not available.

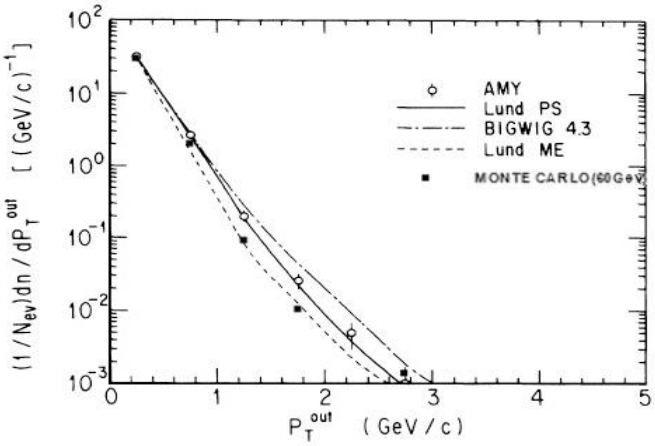

Fig 9: P_T^{out} distributions and predictions of the models.

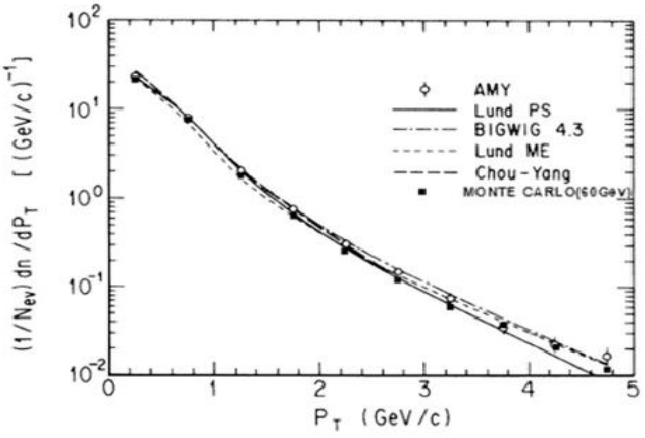

Fig 10: P_T distributions and predictions of the models.

Following parton generation, hadrons are formed according to a string fragmentation scheme. A string is stretched between the final quarks forming a color-singlet system and is allowed to break by forming additional color-string quark pairs. Gluons are treated as kinks on the string between the quark ends with associated energy and momentum, and are therefore attached to two strings to the gluon's double color charge. The longitudinal component of the momenta of the final-state hadrons formed in fragmentation process is distributed according to the symmetric fragmentation function.

$$f(z) = \frac{(1-z)^a}{z} e^{-b m_T^2/z},$$

where m_T is the transverse mass of the hadrons ($m_T^2 = m^2 + P_T^2$) and *z* is the fraction of the primordial parton energy it carries. Each primary quark is assigned a transverse momentum following a Gaussian spectrum $\sim \exp\left(-p_T^2/2\sigma_q^2\right)$. The fragmentation parameters *a*, *b*, and σ_q are relevant to such inclusive global properties as multiplicities and rapidity distributions. These parameters are in addition to the basic model parameters $A_{\overline{MS}}$ and y_{min}.

ISSN 2347-3487

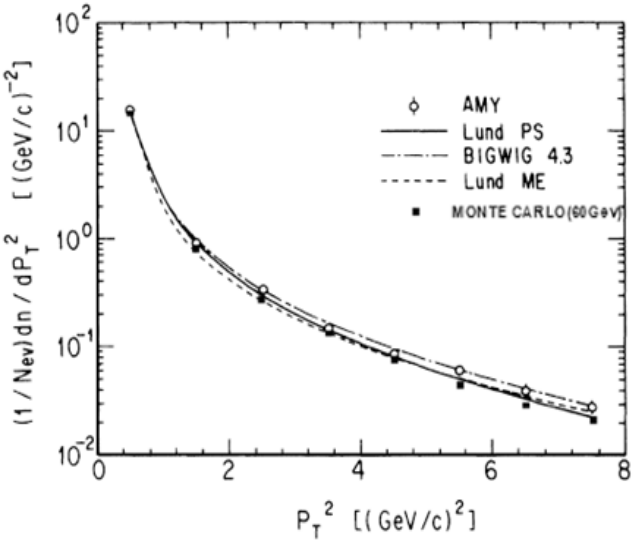

Fig 11: P_T^2 distributions and predictions of the models.

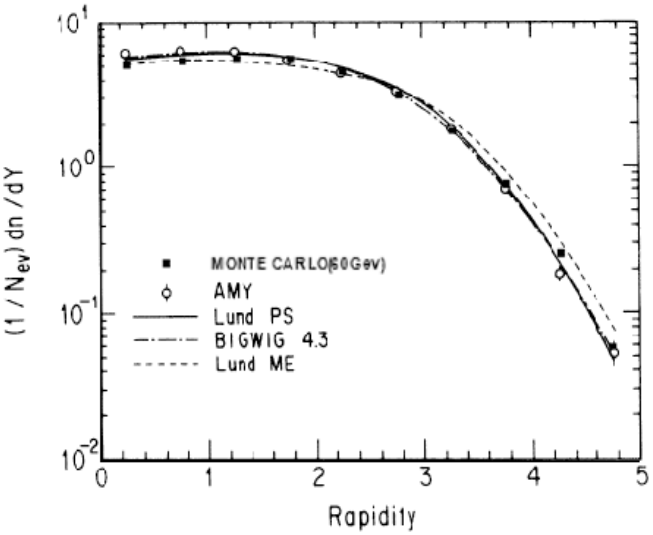

Fig 12: Rapidity distributions and predictions of the models.

4. OBSERVABLES IN ANALYSIS OF MULTIHADRON-EVENT PROPERTIES[1,2]

Events are characterized according to their shape in momentum space by the eigenvalues of the sphericity tensor,

$$S_{\alpha\beta} = \frac{\sum p_{i\alpha} p_{i\beta}}{\sum |p_i|^2},$$

in which $\alpha, \beta = 1,2,3$ and the sum runs over all particles *i* in an event. The eigenvalues Q_1, Q_2, Q_3 (ordered such that $Q_1 < Q_2 < Q_3$ and normalized so that $Q_1 + Q_2 + Q_3 = 1$) and the corresponding principal axes n_1, n_2, n_3 of the momentum ellipsoid are determined for each event. The sphericity axis n_3 defines the events axis and the event plane is given by (n_2, n_3). Because the sphericity tensor uses the momenta of the particles quadratically, the high-momentum particles in an event will contribute more strongly to observables derived from this tensor than to those which use the momenta linearly.

A measure of event structure that uses the linear momenta is the thrust

$$T = \max \frac{\sum |P_{iL}|}{\sum |P_i|},$$

the thrust axis is chosen to maximize $\sum |P_{iL}|$, the sum of the components of the momenta parallel to the thrust axis of all particles in an event. Extreme two-jet events with completely collinear final-state particles would have $T = 1$, and those completely isotropic would have $T = 1/2.$

All observed charged particles, are included in the determination of event shapes, axes, and jet masses. The observables used in our measurement are defined as follows:

(a) The charged-particles rapidity with respect to the thrust axis is defined as $Y = 1/2 \ln\left[(E + P_L)/(E - P_L)\right]$, where *E* is the particle energy and p_L is the component of the momentum parallel to the trust axis.

ISSN 2347-3487

(b) The scaled track momentum $X = 2\mathrm{P}/\sqrt{\mathrm{s}}$ is one common fragmentation variable for charged particles that used in this analysis.

(c) There are several charged-particle transverse momentum variables derived from the sphericity tensor. P_T is the charged-particle momentum transverse to the sphericity axis and P_T^2 is its square. P_T^{in} and P_T^{out} are, respectively, the charged-particle transverse momenta in and out of the event plane, while $\left\langle \mathrm{P}_{\mathrm{T}}^{2\,\mathrm{in}} \right\rangle = \left\langle \mathrm{P}^2 \right\rangle \mathrm{Q}_2$ and $\left\langle \mathrm{P}_{\mathrm{T}}^{2\,\mathrm{out}} \right\rangle = \left\langle \mathrm{P}^2 \right\rangle \mathrm{Q}_1$.

(d) The charged-particle flow is defined as $dn/d\theta$ where θ is the angle between the particle and the sphericity axis. The energy flow $dE/d\theta$ is also used, defined by weighting $dn/d\theta$ by the energies of the charged and neutral particles.

(e) Thrust distributions are also used. The axis perpendicular to the thrust axis with the greatest thrust value is defined to be the major axis, and the sum of the longitudinal momenta with respect to this axis over the sum of momenta is the major value M_2. The minor axis is assigned so as to form an orthonormal system, and the minor value M_3 is the thrust value along this axis. The difference between the major and minor values is the oblateness. These observables use momenta linearly, and are therefore more sensitive to soft particle production than those derived from sphericity analysis.

(f) The sphericity is defined as $\mathrm{S} = \frac{3}{2}(\mathrm{Q}_1 + \mathrm{Q}_2)$. Ideal two-jet events would have $S = 0$, while S would equal unity for completely isotropic events.Aplanarity, $\mathrm{A} = 3/2\mathrm{Q}_1$, and the variables $\mathrm{Q}_{\mathrm{x}} = (1/\sqrt{3})(\mathrm{Q}_3 - \mathrm{Q}_2)$ and $\mathrm{Q}_2 - \mathrm{Q}_1$ are also used.

(g) The event may be divided into hemispheres by the plane perpendicular to the sphericity axis, and the total invariant mass of all particles in each hemisphere calculated. The scaled jet invariant mass squared of each of the hemispheres of an event is a well-behaved quantity in perturbation calculations. The smaller of the two values defines M_{sl}, the mass of the slim jet, and the other defines M_{br}, the mass of the broad jet. The scaled quantities of interest are M_{sl}^2/s , M_{br}^2/s, and $(M_{sl}^2 - M_{br}^2)/s$

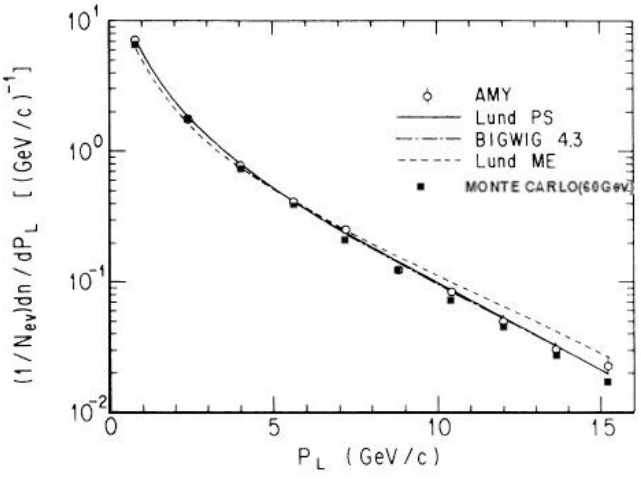

Fig 13: P_L distributions and predictions of the models.

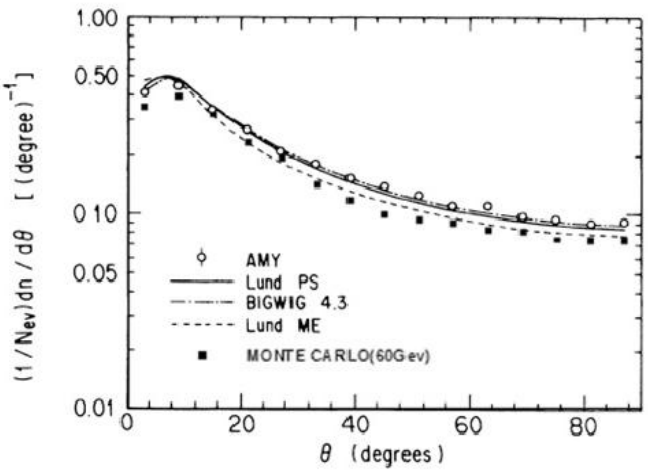

Fig 14: θ distributions and predictions of the models.

5- Comparison of AMY results with different Models

In Figures 1- 14 the data distributions on the AMY data as well as the Monte-Carlo PYTHIA are shown and compared with the predictions of Lund ME, Lund PS, and Webber models. In Figs 7 and 10 we also compare our data for x and P_T distributions with the Chou – Yang parametrization[14]. We observe that in most cases the Lund ME model shows

significant disagreement with the AMY data. On the other hand the Lund parton- shower model gives in general a good description of AMY data, and , of the three model considered, yields the most satisfactory agreement, though with certain discrepancies.

6- Summary

We have studied multihadron events from e^+e^- annihilations for AMY as well as the PHTYIA Monte-Carlo data. Event shape, particle flow and inclusive particle distributions have been measured. We observe that Lund ME shows some large deviations and demonstrates significant difficulties in reproducing the experimental data for most of the event shape distributions. On the other hand, both the Webber and the Lund PS models provide a good description of AMY data. In general the Webber model gives a fairly good description of the P_T^{in} related quantities but reproduces less well the P_T^{out} related distributions. The Lund PS too is in reasonable agreement with P_T^{in} distributions, yet also yields an accurate reproduction of P_T^{out} quantities.

Acknowledgements

This work has funded by the Vice president for Research &Technology of Ferdowsi University of Mashhad, Code 2/15353. This work has also been supported by Payesh research institute of fundamental physics.

Reference:

[1] V.A. Khoze, W. Ochs. Int. J. Mod. Phys. A 12 (1997) 2949.

[2] Yu.L. Dokshitzer, V.S. Fadin and V.A. Khoze, Phys. Lett. B115 (1982) 242

[3] C.P. Fong and B.R. Webber, Nucl. Phys. B355 (1991) 54

[4] D.Gross and F. Wilczek, Phys.Rev . Lett.30,1973;

[5] T.Sjostrand and M.Bengtsson,Comput.Phys. Commun.(1987)

[6] G. Altarelli, Phys. Rep. 81 (1982) 1.

[7] T. Sjostrand, Comp. Phys. Comm. 82 (1994) 74.

[8] B. Anderson et al., Phys. Rep. 97 (1983) 31.

[9] G. Marchesini et al., Comp. Phys. Comm. 67 (1992) 465.

[10] C. Peterson et al., Phys. Rev. D 27 (1983) 105.

[11] ALEPH Collaboration. Physics Reports 294 (1998) l-l 65

[12] PYTHIA 5.7 and JETSET 7.4 Physics and Manual. hep-ph/9508391

[13] Y. K. Li *et al*, AMY Collaboration, *Phys Rev* **D41,**2675 1990.

[14] T.T. Chou and C. N. Yang, Phys. Lett. **B212**, 185 (19980.

[15] JADE Collaboration, W. Bartel et al., Z. Phys. C 25, 231 (1984); 33, 23 (1986).

[16] TASSO Collaboration, W. Braunschweig et al., Phys. Lett. B214, 286 (1988).

[17] AMY Collaboration, I. H. Park et al., Report No. KEK 88-45, 1988.

[18] T. Sjostrand and M. Bengtsson, Compt. Phys. Commun. 43, 367 (1987).

[19] B. Anderson et al., Phys. Rep. 97, 33 (1983).

[20] T. Sjostrand, Int. J. Mod. Phys. A3, 751 (1988).

[21] G. Marchesini and B. Webber, Nucl. Phys. B238, 1 (1984); B. Webber, ibid B238, 492, (1984).

[22] G. Marchesini and B. Webber, Nucl. Phys. B310, 461 (1988).

[23] T. Sjostrand, Comp. Phys. Comm. 39, 347 (1986).

[24] The L3 Collaboration. arXiv:hep-ex/0406049v1 18 Jun 2004, arXiv:hep-ex/0005045v1 29 May 2000, arXiv:hep-ex/0206052v1 20 Jun 2002.